Contribution from the Department of Chemistry and Molecular Structure Center, Indiana University, Bloomington, Indiana 47405, and Department of Chemistry, D-006, University of California at San Diego, La Jolla, California 92093-0506

Preparation and Properties of Models for the Photosynthetic Water Oxidation Center: Spin Frustration in the $[Mn_4O_2(O_2CR)_7(pic)_2]^-$ Anion

Eduardo Libby,[1a] James K. McCusker,[1b] Edward A. Schmitt,[1b] Kirsten Folting,[1c] David N. Hendrickson,*[,1b] and George Christou*[,1a]

Received April 9, 1991

Synthetic procedures are described that allow access to complexes containing the anion $[Mn_4O_2(O_2CR)_7(pic)_2]^-$ (R = Me, Et, Ph; picH = picolinic acid). Reaction mixtures consisting of $Mn(O_2CR)_2$ (R = Me, Ph), RCOOH, pic^-, and $NBu^n_4MnO_4$ in MeCN give deep red solutions from which the products $(NBu^n_4)[Mn_4O_2(O_2CMe)_7(pic)_2]$ (**1**) and $(NBu^n_4)[Mn_4O_2(O_2CPh)_7(pic)_2]$ (**2**) can be obtained in high yield and purity. Complex **1**·MeCN crystallizes in triclinic space group $P\bar{1}$ with (at −158 °C) a = 12.655 (2) Å, b = 18.919 (4) Å, c = 11.951 (2) Å, α = 98.00 (1)°, β = 101.07 (1)°, γ = 77.43 (1)°, Z = 2, and V = 2726.59 Å^3. The structure was solved by direct methods (MULTAN) and refined to values of conventional indices R (R_w) of 7.01% (6.90%) by using 5778 unique reflections with $F > 3\sigma(F)$. The structure of the anion consists of an $[Mn_4(\mu_3\text{-}O)_2]^{8+}$ core with the four Mn atoms disposed in a "butterfly" arrangement and O atoms triply bridging each plane ("wing"). Peripheral ligation is provided by seven μ-AcO^- and two chelating pic^- groups; the overall structure has idealized C_2 symmetry. The anion of **1** bears striking similarity to the cation $[Mn_4O_2(O_2CMe)_7(bpy)_2]^+$ reported previously, showing little structural consequence of the pic-for-bpy substitution. Treatment of $[Mn_3O(O_2CR)_6(py)_3](ClO_4)$ (R = Me, Et) with $Na(pic)\cdot{}^3/_4H_2O$ in MeCN leads to formation of sparingly soluble $Na[Mn_4O_2(O_2CR)_7(pic)_2]$ salts, providing an additional synthetic route to the tetranuclear anions. Complex **1** can be cleanly converted to **2** by treatment with excess PhCOOH in MeCN, demonstrating facile carboxylate exchange with more acidic acids. Variable-temperature, solid-state magnetic susceptibility studies have been performed on complex **1** in the range 5-300 K. The effective magnetic moment, μ_{eff}/Mn_4, decreases gradually from 7.98 μ_B at 300.0 K to 6.35 μ_B at 25.00 K and then decreases more rapidly to 3.28 μ_B at 5.00 K. The data were fit to a theoretical expression derived from the appropriate spin Hamiltonian for a Mn_4O_2 core with C_{2v} symmetry which also included an axial zero-field splitting term $[D(\hat{S}_z^2 - {}^1/_3\hat{S}_T^2)]$ for the S = 3 ground state. The fitting parameters are J_{wb} = −5.3 cm^{-1}, J_{bb} = −24.6 cm^{-1}, g = 1.96, and D = 3.7 cm^{-1} with TIP held constant at 200 × 10^{-6} cgsu; J_{bb} refers to the interaction between the two-body bis(μ-oxide)-bridged Mn^{III} atoms, and J_{wb} refers to the four mono(μ-oxide)-bridged pairs of Mn^{III} atoms. The exchange parameters are very similar to those previously reported for $[Mn_4O_2(O_2CMe)_7(bpy)_2](ClO_4)\cdot 3H_2O$ (J_{wb} = −7.8 cm^{-1}, J_{bb} = −23.5 cm^{-1}), consistent with the structural similarities between the two complexes. The spin frustration present in these $[Mn_4O_2]^{8+}$ complexes is examined in detail. Depending on the magnitudes of J_{wb} and J_{bb}, different ground states are found. The presence of μ_3-oxide-bridged Mn^{III}_4 units in these complexes causes frustration in the spin alignment at each Mn ion. The proton NMR spectral data are reported for complex **1** in $CDCl_3$, CD_3CN, and $(CD_3)_2SO$. The spectra in all three solvents are very similar, supporting retention of the solid-state structure of the anion of **1** in good donor solvents. The only major influence of the pic-for-bpy substitution is to be found in the redox properties investigated by cyclic voltammetry. Complexes **1** and **2** display a quasi-reversible oxidation in CH_2Cl_2 at +0.52 and +0.54 V vs ferrocene, respectively. The latter is to be contrasted with the value of +0.87 V found previously for $[Mn_4O_2(O_2CPh)_7(bpy)_2](ClO_4)$, showing that oxidation to the $3Mn^{III},Mn^{IV}$ oxidation level becomes easier when bpy is replaced by pic^-.

Introduction

Intense effort is currently being concentrated on elucidating the nature and mode of action of the site responsible for water oxidation/oxygen evolution within the photosynthetic apparatus of green plants and cyanobacteria.[2] A variety of studies indicate this site to be an Mn_4 aggregate operating on the donor side of photosystem II (PSII). The four Mn atoms are essential for activity and appear to be in close proximity to each other, either as a tetranuclear cluster, a trinuclear cluster close to a mononuclear site, or a pair of closely spaced dinuclear clusters. Other available data include the following: the Mn···Mn separations are of two types (2.72 (3) and ~3.3 Å); the metals are bridged by oxides (O^{2-}) or hydroxides; and ligation is by O- and/or N-based groups from amino acid side chains (tyrosine phenoxide, histidine imidazole, aspartate/glutamate carboxylate).[2,3] The complete Mn_4 assembly cycles between five oxidation levels during turnover (S_0–S_4), the most oxidized state, S_4, being unstable and converting back to S_0 with evolution of O_2. A "superreduced" state, S_{-1}, is also accessible under certain conditions but is not apparently involved in the catalytic cycle.[4]

Before an understanding of the water oxidation center (WOC) may be said to have been achieved, it is necessary as a minimum requirement to be able to answer the following: (i) What is the structure of the Mn_4 assembly at the various S_n states? (ii) How are the substrate (H_2O) molecules bound? (iii) What is the mechanism by which the substrate molecules are deprotonated and reductively eliminated as O_2? It is indeed possible that the above are really the same question in different forms. We recently reported the synthesis of the complexes $Mn_4O_2(O_2CR)_6(bpy)_2$ and $[Mn_4O_2(O_2CR)_7(bpy)_2]^{0,+}$ containing the $[Mn_4O_2]^{n+}$ (n = 6–8) core with the metals disposed in either a planar or a nonplanar ("butterfly") fashion.[5,6] For a variety of reasons, we considered these complexes to be attractive candidates for structural models of the S_{-1}, S_0, and S_1 states of the WOC. We have also reported complexes containing the distorted cubane $[Mn_4O_3Cl]^{6+}$ core[7] and proposed that these $3Mn^{III},Mn^{IV}$ species might be models for the S_2 state. It was suggested that the third O^{2-} required for con-

(1) (a) Chemistry Department, Indiana University. (b) University of California. (c) Molecular Structure Center, Indiana University.

(2) (a) Govindjee; Kambara, T.; Coleman, W. *Photochem. Photobiol.* **1985**, *42*, 187. (b) Dismukes, G. C. *Ibid.* **1986**, *43*, 99. (c) Renger, G. *Angew. Chem., Int. Ed. Engl.* **1987**, *26*, 643. (d) Brudvig, G. W. *J. Bioenerg. Biomembr.* **1987**, *19*, 91. (e) Babcock, G. T. In *New Comprehensive Biochemistry*; Amesz, J., Ed.; Elsevier: Dordrecht, Holland, 1987; Vol. 15, pp 125–158. (f) Pecoraro, V. L. *Photochem. Photobiol.* **1988**, *48*, 249. (g) Vincent, J. B.; Christou, G. *Adv. Inorg. Chem.* **1989**, *33*, 197. (h) Ghanotakis, D.; Yocum, C. F. *Annu. Rev. Plant Physiol. Mol. Biol.* **1990**, *41*, 255.

(3) (a) Guiles, R. D.; Yachandra, V. K.; McDermott, A. E.; Cole, J. L.; Dexheimer, S. L.; Britt, R. D.; Sauer, K.; Klein, M. P. *Biochemistry* **1990**, *29*, 486 and references therein. (b) Guiles, R. D.; McDermott, A.; Yachandra, V. K.; Cole, J. L.; Dexheimer, S. L.; Britt, R. D.; Wieghardt, K.; Bossek, U.; Sauer, K.; Klein, M. P. *Ibid.* **1990**, *29*, 471. (c) George, G. N.; Prince, R. C.; Cramer, S. P. *Science* **1989**, *243*, 789. (d) Penner-Hahn, J. E.; Fronko, R. M.; Pecoraro, V. L.; Yocum, C. F.; Betts, S. D.; Bowlby, N. R. *J. Am. Chem. Soc.* **1990**, *112*, 2549.

(4) (a) Pistorius, E. K.; Schmid, G. H. *Biochem. Biophys. Acta* **1987**, *890*, 352. (b) Bader, K. P.; Thibault, P.; Schmid, G. H. *Z. Naturforsch., C: Biosci.* **1983**, *38C*, 778. (c) Velthuys, B.; Kok, B. *Biochim. Biophys. Acta* **1978**, *502*, 211.

(5) Vincent, J. B.; Christmas, C.; Chang, H.-R.; Li, Q.; Boyd, P. D. W.; Huffman, J. C.; Hendrickson, D. N.; Christou, G. *J. Am. Chem. Soc.* **1989**, *111*, 2086.

(6) Christou, G. *Acc. Chem. Res.* **1989**, *22*, 328.

(7) (a) Bashkin, J. S.; Streib, W. E.; Huffman, J. C.; Chang, H.-R.; Hendrickson, D. N.; Christou, G. *J. Am. Chem. Soc.* **1987**, *109*, 6502. (b) Li, Q.; Vincent, J. B.; Libby, E.; Chang, H.-R.; Huffman, J. C.; Boyd, P. D. W.; Christou, G.; Hendrickson, D. N. *Angew. Chem., Int. Ed. Engl.* **1988**, *27*, 1731.

0020-1669/91/1330-3486$02.50/0

version of Mn_4O_2 to Mn_4O_3Cl might arise from substrate (H_2O) molecules; a mechanistic scheme for the catalytic cycle based on these structures and the suggested substrate-incorporation step has been proposed.[8]

In extending the above work, it was considered important to reproduce in the model complexes the ligation environment around the native Mn_4 unit as closely as possible. Even if the complexes were to prove structurally noncongruent with the Mn_4 site of the WOC, it is felt that observed properties and chemistry of synthetic materials with the correct ligation might nevertheless be informative and perhaps comparable with those of the WOC Mn_4 unit. The use of bpy (2,2'-bipyridine) was important in allowing initial access to $[Mn_4O_2]$ complexes and as such was a means to an end. However, recent reports have suggested that the number of nitrogen-based (histidine) ligands on the metals either to be zero or to be at the level of $1/Mn_4$ or $2/Mn_4$.[9] It thus seemed that the two bpy groups in our complexes result in too high a ratio of N:Mn_4, and we have sought to redress the situation. We herein report the results of this effort, the successful replacement of bpy by picolinate (pic^-) to give an $[Mn_4O_2]^{8+}$ complex with the number of nitrogen-based ligands halved and the carboxylate ligation consequently increased. We also assess the effect of this substitution on structural parameters and physicochemical properties. Furthermore, the electronic structure of $[Mn_4O_2]^{8+}$ complexes is examined in detail. Different competing antiferromagnetic exchange interactions within each $[Mn_4O_2]^{8+}$ complex lead to spin frustration and consequently an intermediate-spin ground state. Spin frustration can lead to a variety of intermediate-spin (S = 1, 2, or 3) ground states depending on the relative values of the parameters characterizing the pairwise exchange interactions in a $[Mn_4O_2]^{8+}$ complex.

Experimental Section

Syntheses. All manipulations were performed under aerobic conditions, using materials as received; water was distilled in-house. Trinuclear $[Mn_3O]$ complexes were available from previous work.[10] $NBu^n_4MnO_4$ was prepared as described.[11] *Warning*! Appropriate care should be taken in the use of $NBu^n_4MnO_4$, and readers are referred to the detailed warning given elsewhere.[11]

Na(pic)·$^3/_4H_2O$. A solution of picolinic acid (5.0 g, 40 mmol) in H_2O (6 cm^3) was diluted with EtOH (50 cm^3), followed by addition of a solution of NaOH (1.60 g, 40 mmol) in H_2O (5 cm^3). To the resulting clear solution was added Et_2O (60 cm^3) and the precipitated white solid collected by filtration, washed with 1:1 EtOH/Et_2O (2 × 50 cm^3) and Et_2O (3 × 50 cm^3), and dried in vacuo. The yield was 4.8 g (76%). Anal. Calcd for $C_6H_{5.5}NO_{2.75}Na$: C, 45.43; H, 3.50; N, 8.83; Na, 14.50. Found: C, 46.0; H, 3.4; N, 8.9; Na, 14.3.

$Mn(O_2CPh)_2·2H_2O$. A slurry of $MnCO_3$ (4.1 g, 36 mmol) and benzoic acid (8.8 g, 72 mmol) in H_2O (200 cm^3) was stirred at 50 °C for 24 h. The mixture was filtered and the filtrate concentrated to ~20 cm^3 in vacuo. Overnight storage at 5 °C gave white crystals, which were collected by filtration, washed with H_2O (20 cm^3) and Et_2O (5 × 50 cm^3), and dried in air. The yield was 7.2 g (60%). Anal. Calcd for $C_{14}H_{14}O_6Mn$: C, 50.47; H, 4.24; Mn, 16.49. Found: C, 50.7; H, 4.2; Mn, 16.9.

$Mn(O_2CCD_3)_2·4H_2O$. A suspension of $MnCO_3$ (1.90 g, 16.5 mmol) in water (5 cm^3) and CD_3COOD (1.00 g, 16.1 mmol) was stirred for 24 h at ambient temperature. The mixture was filtered and the filtrate evaporated to dryness at 40 °C in vacuo. The resulting pink crystals were collected and further dried in vacuo. The yield was 1.2 g (60% based on CD_3COOD).

$(NBu^n_4)[Mn_4O_2(O_2CMe)_7(pic)_2]$ (1). To a stirred solution of Mn$(O_2CMe)_2·4H_2O$ (0.78 g, 3.2 mmol), glacial acetic acid (1.0 cm^3, 17 mmol), and NBu^n_4Cl (1.2 g, 4.0 mmol) in MeCN (70 cm^3) was slowly added solid $NBu^n_4MnO_4$ (0.29 g, 0.80 mmol) in small portions to give a deep brown solution. To this was added a solution of Na(pic)·$^3/_4H_2O$ (0.32 g, 2.0 mmol) in H_2O (0.50 cm^3) to give a deep red solution and some greenish white precipitate. The latter was removed by filtration and the filtrate evaporated in vacuo to yield a red microcrystalline solid. This was washed with MeCN (3 × 2 cm^3), 1:1 MeCN/Et_2O (3 × 4 cm^3), and Et_2O (5 cm^3) and dried in air. The solid was purified by dissolution in MeCN (30 cm^3) followed by filtration, addition of Et_2O (50 cm^3) to the filtrate, and overnight storage of the solution at −15 °C. The resulting deep red crystals were collected by filtration, washed with 1:1 MeCN/Et_2O (3 × 7 cm^3) and Et_2O (3 × 3 cm^3), and dried in air. The yield was 0.53 g (46% based on Mn). Crystals suitable for crystallography were grown by vapor diffusion of Et_2O into a concentrated MeCN solution of the complex; they were found to rapidly lose solvent and were therefore kept in contact with their mother liquor until they were selected and rapidly transferred to the diffractometer cold stream for characterization. The dried solid analyzed for no solvent of crystallization. Anal. Calcd for $C_{42}H_{65}N_3O_{20}Mn_4$: C, 43.80; H, 5.69; N, 3.65; Mn, 19.08. Found: C, 43.7; H, 5.7; N, 3.6; Mn, 19.5. IR spectrum, cm^{-1} (Nujol mull): 3400 (w, br), 3095 (w), 3074 (w), 1676 (s), 1610 (s), 1559 (m), 1399 (s), 1335 (s), 1325 (s), 1292 (m), 1262 (w), 1161 (m), 1049 (w), 1020 (w), 932 (w), 884 (w), 858 (m), 771 (w), 763 (w), 714 (m), 679 (m), 667 (s), 648 (s), 609 (m), 463 (m). Magnetic moment per Mn_4 in $CDCl_3$ solution (Evans method): 8.2 ± 0.2 μ_B at 25.0 °C.

The deuterioacetate version of complex **1**, $(NBu^n_4)[Mn_4O_2(O_2CCD_3)_7(pic)_2]$, was prepared in an analogous manner employing $Mn(O_2CCD_3)_2·4H_2O$ and CD_3COOD.

$(NBu^n_4)[Mn_4O_2(O_2CPh)_7(pic)_2]$ (2). To a stirred solution of Mn$(O_2CPh)_2·2H_2O$ (1.33 g, 4.0 mmol) and PhCOOH (0.85 g, 7.0 mmol) in MeCN (100 cm^3) was slowly added solid $NBu^n_4MnO_4$ (0.36 g, 1.0 mmol) in small portions to give a deep brown solution. To this was added a solution of Na(pic)·$^3/_4H_2O$ (0.40 g, 2.5 mmol) in H_2O (0.50 cm^3). An off-white precipitate was removed by filtration. The dark red filtrate was concentrated in vacuo to an oil and redissolved in CH_2Cl_2 (20 cm^3), and the solution was filtered. The filtrate was diluted with Et_2O (10 cm^3) and layered with 2:1 Et_2O/hexanes (30 cm^3). After a few days, dark red crystals formed, together with small amounts of a white solid. Purification was effected by repeating the above crystallization procedure. The resulting dark red crystals were collected by filtration, washed with Et_2O (3 × 10 cm^3), and dried in air. The yield was 0.50 g (25%). Anal. Calcd for $C_{77}H_{79}N_3O_{20}Mn_4$: C, 58.30; H, 5.02; N, 2.65; Mn, 13.85. Found: C, 58.2; H, 5.0; N, 2.5; Mn, 14.1. IR spectrum, cm^{-1} (Nujol mull): 3057 (w), 1674 (s), 1605 (s), 1570 (s), 1329 (s), 1291 (s), 1258 (m), 1173 (m), 1155 (m), 1067 (w), 1047 (m), 1026 (m), 856 (w), 839 (w), 768 (w), 716 (s), 688 (s), 664 (s), 652 (s), 611 (m), 467 (s). The crystals were poor diffractors of X-rays.

Conversion of 1 to 2. A solution of complex **1** (0.58 g, 0.50 mmol) in MeCN (40 cm^3) was treated with PhCOOH (0.43 g, 3.5 mmol). After 2 h, the clear dark red solution was concentrated to an oil in vacuo and redissolved in CH_2Cl_2 (10 cm^3), and the mixture was layered with 2:1 Et_2O/hexanes (30 cm^3). After several days, the resulting dark red crystals were collected by filtration, washed with 5:1 Et_2O/CH_2Cl_2 (4 × 10 cm^3), and dried in air. The yield was 0.50 g (67%). The IR spectrum was identical with that of authentic material. Anal. Calcd for $C_{77}H_{79}N_3O_{20}Mn_4$: C, 58.30; H, 5.02; N, 2.65; Mn, 13.85. Found: C, 57.8; H, 5.1; N, 2.5; Mn, 13.85.

$Na[Mn_4O_2(O_2CMe)_7(pic)_2]·^1/_2MeCN·^1/_2H_2O$ (3). A brown solution of $[Mn_3O(O_2CMe)_6(py)_3](ClO_4)$ (0.87 g, 1.0 mmol) in MeCN (50 cm^3) and glacial acetic acid (5 cm^3) was treated with a solution of Na(pic)·$^3/_4H_2O$ (0.30 g, 1.9 mmol) in H_2O (0.4 cm^3) to give a deep red solution. The flask was left undisturbed for 48 h to give large dark red crystals. These were collected by filtration, washed with MeCN (2 × 10 cm^3), and dried in air. The yield was 0.43 g (61%). Anal. Calcd for $C_{27}H_{31.5}N_{2.5}O_{20.5}NaMn_4$: C, 33.72; H, 3.30; N, 3.64; Na, 2.39; Mn, 22.85. Found: C, 33.6; H, 3.4; N, 4.2; Na, 2.5; Mn, 23.3. IR spectrum, cm^{-1} (Nujol mull): 3500 (m, br), 3090 (w), 3069 (w), 2245 (w), 1684 (m), 1597 (s), 1329 (s), 1292 (s), 1264 (m), 1159 (m), 1051 (m), 1030 (m), 936 (w), 862 (m), 768 (m), 716 (m), 671 (s), 613 (s), 468 (m).

$Na[Mn_4O_2(O_2CEt)_7(pic)_2]·^3/_4H_2O$ (4). A solution of $[Mn_3O(O_2CEt)_6(py)_3](ClO_4)$ (0.96 g, 1.0 mmol) in MeCN (50 cm^3) was treated with a solution of Na(pic)·$^3/_4H_2O$ (0.29 g, 1.8 mmol) in H_2O (0.4 cm^3) to slowly give a red microcrystalline precipitate. This was collected by filtration, washed with MeCN (3 × 5 cm^3), and dried in air. The yield was 0.90 g. The filtrate slowly produced more product as dark red crystals overnight, isolated as above. The combined yield was 0.99 g (90%). Anal. Calcd for $C_{33}H_{44.5}N_2O_{20.75}NaMn_4$: C, 37.97; H, 4.30; N, 2.68; Mn, 21.05. Found: C, 37.6; H, 4.0; N, 2.8; Mn, 21.5. IR spectrum, cm^{-1} (Nujol mull): 3424 (w, br), 3082 (w), 3069 (w), 1690 (s), 1603 (s), 1527 (m), 1395 (s), 1323 (s), 1285 (s), 1244 (m), 1153 (m), 1082 (m), 1051 (m), 1028 (w), 1010 (w), 860 (m), 825 (w), 810 (w), 779 (m), 716 (m), 693 (m), 673 (s), 656 (s), 613 (m), 471 (m).

X-ray Crystallography. Data for complex **1** were collected on a Picker four-circle diffractometer at −158 °C; details of the diffractometry, low-temperature facilities, and computational procedures employed by the Molecular Structure Center are available elsewhere.[12] Data col-

(8) Christou, G.; Vincent, J. B. *Biochim. Biophys. Acta* **1988**, *895*, 259.
(9) (a) Tamura, N.; Ikeuchi, M.; Inoue, Y. *Biochim. Biophys. Acta* **1989**, *973*, 281. (b) Andreasson, L.-E. *Ibid.* **1989**, *973*, 465.
(10) Vincent, J. B.; Chang, H.-R.; Folting, K.; Huffman, J. C.; Christou, G.; Hendrickson, D. N. *J. Am. Chem. Soc.* **1987**, *109*, 5703.
(11) Vincent, J. B.; Folting, K.; Huffman, J. C.; Christou, G. *Inorg. Chem.* **1986**, *25*, 996.

Table I. Crystallographic Data for Complex **1**·MeCN

formula	$C_{44}H_{68}N_4O_{20}Mn_4$
M_r	1192.8
cryst system	triclinic
space group	$P\bar{1}$ (No. 2, C_i^1)
temp, °C	−158
a, Å	12.655 (2)[a]
b, Å	18.919 (4)
c, Å	11.951 (2)
α, deg	98.00 (1)
β, deg	101.07 (1)
γ, deg	77.43 (1)
V, Å^3	2726.59
Z	2
cryst dimens, mm	0.32 × 0.40 × 0.34
λ (Mo Kα),[b] Å	0.71069
abs coeff, cm^{-1}	9.404
scan speed, deg/min	8.0
scan width, deg	1.8 + dispersion
data collcd	$6° \le 2\theta \le 45°$
no. of total data	8010
no. of unique data	7147
averaging R[c]	0.046
no. of obsd data	5778, $F > 3\sigma(F)$
R,[d] %	7.01
R_w,[e] %	6.90
goodness of fit[f]	1.287

[a] 92 reflections. [b] Graphite monochromator. [c] 755 reflections measured more than once. [d] $R_f = \sum||F_o| - |F_c||/\sum|F_o|$. [e] $R_w = [\sum w(|F_o| - |F_c|)^2/\sum w|F_o|^2]^{1/2}$ where $w = 1/\sigma^2(|F_o|)$. [f] Goodness of fit = $[\sum w(|F_o| - |F_c|)^2/(N_{obsns} - N_{params})]^{1/2}$.

lection parameters are collected in Table I. A systematic search of a limited hemisphere of reciprocal space located a set of diffraction maxima with no symmetry or systematic absences. The maxima were indexed by using a triclinic lattice, and the space group $P\bar{1}$ was confirmed by the subsequent solution and refinement of the structure. Four standard reflections showed no systematic variation during data collection. Following usual data reduction and averaging of equivalent reflections, a unique set of 7147 reflections was obtained, of which 5778 reflections were considered observed ($F > 3.0\sigma(F)$). No absorption correction was deemed necessary. The structure was solved by a combination of direct methods (MULTAN) and Fourier techniques and refined by a full-matrix least-squares approach. The Mn atoms were located in the initial E map, and the remaining non-hydrogen atoms were located in successive difference Fourier maps, including those of one MeCN solvent molecule. All non-hydrogen atoms were refined with anisotropic thermal parameters. In the latter stages, most of the hydrogen atoms were visible in a difference Fourier map; due to the large number of independent atoms, however, hydrogen atoms were placed in idealized positions and included in the final refinement cycles as fixed contributors, except for the MeCN hydrogen atoms, which were not included. The final difference Fourier map was essentially featureless except for one peak of 2.15 e/Å^3 near the MeCN atoms, indicating some disorder; these atoms also have large thermal parameters, particularly the nitrogen. No attempt to model the disorder was considered warranted. The next largest peak was 0.72 e/Å^3. Final values of R and R_w are listed in Table I. Selected fractional coordinates and isotropic thermal parameters are given in Table II.

Other Measurements. Variable-temperature magnetic susceptibility data were recorded on a polycrystalline sample of complex **1** with a VTS Model 900 SQUID susceptometer (Bti, Inc., San Diego, CA) in an applied magnetic field of 10.00 kG. Diamagnetic corrections were estimated from Pascal's constants and subtracted from the experimental data to obtain the molar paramagnetic susceptibility values.[13] The latter were fit to the appropriate theoretical expression by means of a relative-error minimization computer program.[14] Infrared (Nujol mull) and electronic solution spectra were recorded on Nicolet 510P and Hewlett-Packard 8452A spectrophotometers, respectively. ^{1}H NMR spectra were recorded on a Varian XL-300 spectrometer. Chemical shifts are quoted on the δ scale (shifts downfield are positive). Cyclic voltammetry was performed by using an IBM Model EC 225 voltammetric analyzer, a PAR Model 175 Universal Programmer, and a standard three-electrode assembly (glassy-carbon working, Pt-wire auxiliary, SCE reference) with 0.1 M $NBu^n_4ClO_4$ as supporting electrolyte. No iR compensation was employed. Quoted $E_{1/2}$ values are vs the ferrocene/ferrocenium couple under the same conditions.

Table II. Selected Fractional Coordinates (×10^4) and Isotropic Thermal Parameters (×10) for Complex **1**

atom	x	y	z	B_{iso}, Å^2
Mn1	8527 (1)	3170 (1)	3959 (1)	20
Mn2	7949 (1)	1737 (1)	2212 (1)	18
Mn3	10402 (1)	2054 (1)	3720 (1)	18
Mn4	10271 (1)	2744 (1)	6405 (1)	20
O5	8917 (3)	2316 (2)	2980 (4)	20
O6	9908 (4)	2790 (2)	4847 (4)	20
O7	7203 (4)	3627 (3)	2959 (4)	25
C8	6501 (6)	3344 (4)	2228 (6)	22
O9	6571 (4)	2683 (2)	1909 (4)	22
C10	5523 (6)	3885 (4)	1730 (7)	29
O11	9283 (4)	796 (2)	2160 (4)	22
C12	10257 (6)	778 (4)	2099 (6)	23
O13	10799 (4)	1280 (3)	2540 (4)	21
C14	10869 (6)	145 (4)	1435 (7)	26
O15	11964 (4)	1877 (3)	4416 (4)	24
C16	12418 (6)	1935 (4)	5463 (6)	19
O17	11941 (4)	2163 (2)	6297 (4)	23
C18	13633 (6)	1691 (5)	5693 (7)	30
O19	8689 (4)	3446 (3)	6750 (4)	26
C20	8040 (6)	3894 (4)	6132 (7)	27
O21	8136 (4)	3968 (3)	5113 (4)	24
C22	7068 (8)	4357 (6)	6567 (9)	52
O23	7463 (4)	2606 (3)	4656 (4)	25
C24	7187 (5)	2010 (4)	4401 (6)	22
O25	7371 (4)	1566 (2)	3519 (4)	21
C26	6552 (6)	1768 (4)	5165 (7)	25
O27	9386 (4)	3774 (3)	3158 (4)	23
C28	10271 (5)	3521 (4)	2765 (6)	20
O29	10809 (4)	2883 (2)	2804 (4)	21
C30	10719 (6)	4055 (4)	2249 (7)	27
O31	10122 (4)	1248 (2)	4748 (4)	22
C32	9742 (6)	1317 (3)	5652 (6)	21
O33	9734 (4)	1866 (2)	6424 (4)	24
C34	9259 (6)	711 (4)	5921 (7)	25
N35	8281 (5)	1888 (3)	655 (5)	22
C36	7678 (5)	1577 (4)	9767 (7)	21
C37	7697 (6)	1668 (4)	8654 (7)	26
C38	8368 (7)	2109 (5)	−1562 (7)	35
C39	9027 (7)	2409 (5)	−629 (7)	37
C40	8971 (7)	2309 (4)	463 (7)	31
C41	6981 (5)	1105 (4)	113 (6)	20
O42	7012 (3)	1154 (2)	1217 (4)	17
O43	6464 (4)	734 (3)	9389 (4)	25
N44	10944 (5)	3664 (3)	6625 (5)	22
C45	11380 (6)	3829 (4)	7709 (6)	22
C46	11972 (6)	4374 (4)	8031 (7)	25
C47	12092 (6)	4771 (4)	7183 (7)	28
C48	11624 (6)	4608 (4)	6054 (7)	28
C49	11054 (6)	4049 (4)	5807 (7)	28
C50	11194 (6)	3351 (4)	8552 (7)	24
O51	10720 (4)	2818 (3)	8054 (4)	25
O52	11470 (4)	3474 (3)	9583 (4)	29

Results

Syntheses. In an earlier report,[5] we described the use of bpy to prepare the tetranuclear complexes $Mn_4O_2(O_2CMe)_6(bpy)_2$ and $[Mn_4O_2(O_2CR)_7(bpy)_2]$.[0,+] These materials were obtained either by treating the trinuclear complexes $[Mn_3O(O_2CR)_6L_3]^{0,+}$ (L = py, H_2O) with bpy or by direct synthesis involving a comproportionation reaction between Mn^{II} and $NBu^n_4MnO_4$ in the presence of RCOOH and bpy. Both procedures gave high yields although the former procedure was employed more routinely. It was decided to screen both procedures when attempts to make picolinate-ligated complexes were initiated, and we have found that both procedures do indeed give the target products. Thus, a MeCN reaction mixture containing $Mn(O_2CMe)_2$, $NBu^n_4MnO_4$, MeCOOH, NBu^n_4Cl, and Na(pic) gave a dark red solution from which pure, highly crystalline $(NBu^n_4)[Mn_4O_2(O_2CMe)_7(pic)_2]$ (**1**) was obtained with minimal workup in good yield (46%). The deuterated version of **1** and the corresponding benzoate complex $(NBu^n_4)[Mn_4O_2(O_2CPh)_7(pic)_2]$ (**2**) were obtained in an analo-

(12) Chisholm, M. H.; Folting, K.; Huffman, J. C.; Kirkpatrick, C. C. *Inorg. Chem.* **1984**, *23*, 1021.
(13) *Theory and Applications of Molecular Paramagnetism*; Boudreaux, E. A., Mulay, L. N., Eds.; Wiley: New York, 1976.
(14) Schmitt, E. A. Unpublished results.

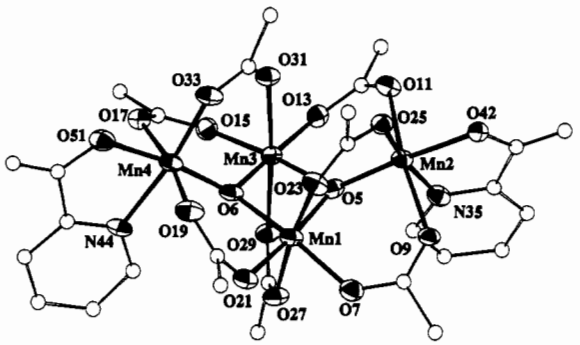

Figure 1. ORTEP diagram for the anion of complex **1**. The carbon atoms are deemphasized and shown as spheres of arbitrary size; they are labeled consecutively from N and O atoms.

gous manner. The Mn^{II}:Mn^{VII} ratio employed was 4:1, as required for a desired Mn^{III}_4 product based on eq 1. The convenient nature

$$4Mn^{2+} + Mn^{7+} \rightarrow {}^5/_4Mn_4{}^{3+} \quad (1)$$

of these reactions, the good (nonoptimized) yields of product, and the absence of intractable, polymeric manganese oxides/hydroxides (that so often plague aqueous $KMnO_4$ reactions) further support our previous assertion[5,11] that $NBu^n_4MnO_4$ is an extremely useful new reagent for inorganic syntheses.

The parallel investigation of the second procedure also led to the desired anionic products in good yield; treatment of MeCN solutions of $[Mn_3O(O_2CR)_6(py)_3](ClO_4)$ (R = Me, Et) with Na(pic) gave dark red solutions from which the sparingly soluble Na^+ salts precipitated in high yields. We had hoped to structurally characterize either the R = Me (**3**) or the R = Et (**4**) complex to ascertain the mode of Na^+ interactions with the anion but were thwarted on numerous occasions by twinning problems. In addition, we did not feel it necessary to seek metathesis methods of converting the Na^+ salts to the more soluble $NBu^n_4{}^+$ salts, given that the convenience and success of the direct synthesis method for the latter using $NBu^n_4MnO_4$ had by now been established.

The $[Mn_4O_2(O_2CMe)_7(pic)_2]^-$ anion of **1** has been found to undergo facile carboxylate exchange with more acidic PhCOOH, completely analogous to the behavior of $[Mn_4O_2(O_2CMe)_7(bpy)_2]^+$.[5] Thus, treatment of **1** in MeCN with a slight excess of PhCOOH leads to clean, high-yield isolation of complex **2** (eq 2). We have commented elsewhere[5,8] on the potential applicability

$$[Mn_4O_2(O_2CMe)_7(pic)_2]^- + 7PhCOOH \rightarrow [Mn_4O_2(O_2CPh)_7(pic)_2]^- + 7MeCOOH \quad (2)$$

of such carboxylate-exchange reactions for extruding biological $Mn/O/RCO_2^-$ units from the native site using a more acidic carboxylic acid (benzoic acid or, better, a water-soluble derivative).

Description of Structure. An ORTEP projection of the anion of complex **1** is given in Figure 1; crystallography data and pertinent bond distances and angles are listed in Tables I and III, respectively.

Complex **1** crystallizes in triclinic space group $P\bar{1}$ with the asymmetric unit containing the complete anion, the $NBu^n_4{}^+$ cation, and one MeCN solvate molecule; the latter two will not be further discussed. The anion possesses a now-familiar Mn_4O_2 core with a "butterfly" structure. Mn1 and Mn3 occupy "body" or "backbone" positions, and Mn2 and Mn4 occupy the "wing-tip" positions; O5 and O6 triply bridge each Mn_3 wing. The structure can thus be considered as two Mn_3O triangular units joined together by edge-sharing with a dihedral angle of 134.98°. Unlike the Mn_3O complexes, however, the μ_3-O atoms do not lie in the Mn_3 planes, but slightly below them (as viewed in Figure 1). Peripheral ligation is by seven bridging AcO^- and two chelating pic^- groups, giving six-coordination at each Mn^{III} center and distorted octahedral geometry. The molecule has idealized C_2 symmetry. All metal centers show clear evidence of Jahn–Teller (JT) distortions, as expected for high-spin octahedral d^4 Mn^{III}, and the axially elongated sites are all occupied by carboxylate oxygen atoms. The pic^- ligands are disposed with their carboxylate

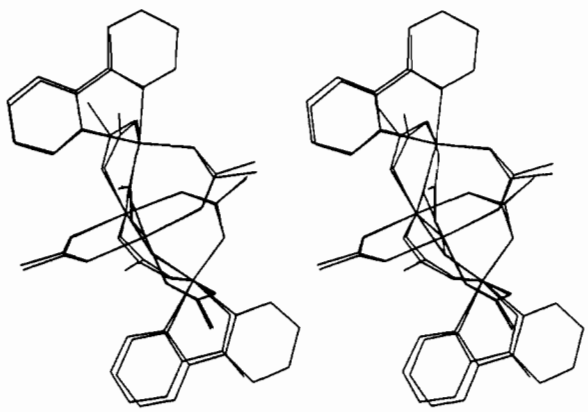

Figure 2. Computer-generated best fit stereoview of the anion of **1** and $[Mn_4O_2(O_2CMe)_7(bpy)_2]^+$ showing the near-superimposability of their inner portions.

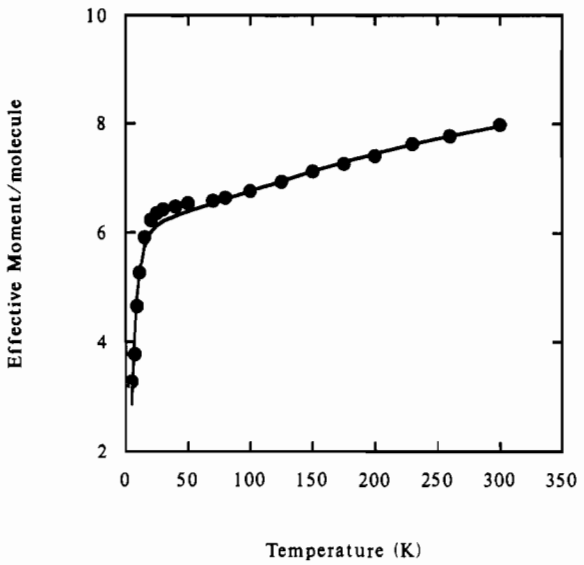

Figure 3. Plot of the effective magnetic moment, μ_{eff}/Mn_4, vs temperature for $(NBu^n_4)[Mn_4O_2(O_2CMe)_7(pic)_2]$ (**1**) in an applied field of 10.00 kG. The solid line represents the best fit of the data to the theoretical equation. See the text for fitting parameters.

oxygen atoms trans to the bridging oxide atoms; the Mn2–O42 and Mn4–O51 bond lengths (1.924 (5) and 1.937 (5) Å, respectively) are comparable to the other (non-JT elongated) Mn–carboxylate bonds (1.931 (5)–1.968 (5) Å). Only one carboxylate, the unique one bridging the two "body" Mn atoms, has *both* its oxygen atoms (O27 and O29) occupying JT axially elongated positions. The butterfly disposition of the Mn_4 core leads to two, distinctly different, types of Mn···Mn separation. The central Mn1···Mn3 separation (2.842 (2) Å) is much shorter than the four edge separations (3.308 (2)–3.406 (2) Å). This is in accord with the number of bridging oxides; we have reviewed elsewhere the Mn···Mn separations in oxide-bridged systems and commented that Mn···Mn separations are ~2.7–2.8 Å if bridged by *two* oxides and ~3.3 Å if bridged by only one.[15]

The structure of the anion of **1**, as detailed in the discussion above and in Table III, shows remarkable similarity to that of $[Mn_4O_2(O_2CMe)_7(bpy)_2]^+$.[5] Rather than tabulate comparative structural parameters, we present in Figure 2 a stereopair showing a computer-generated best fit of the two tetranuclear ions. Clearly evident is the near superimposition of the central portions, with noticeable discrepancies only at the outer positions of the peripheral ligands. Obviously, the replacement of bpy by pic^- has little structural effect.

(15) Christou, G.; Vincent, J. B. In *ACS Symposium Series 372*; Que, L., Ed.; American Chemical Society: Washington, DC, 1988; Chapter 12, pp 238–255.

Table III. Selected Interatomic Distances (Å) and Angles (deg) for Complex **1**

a. Distances

Mn1···Mn2	3.308 (2)	Mn1···Mn3	2.842 (2)
Mn1···Mn4	3.386 (2)	Mn2···Mn3	3.406 (2)
Mn3···Mn4	3.313 (2)		
Mn1–O5	1.890 (5)	Mn3–O5	1.908 (4)
Mn6–O6	1.910 (5)	Mn3–O6	1.888 (5)
Mn1–O7	1.968 (5)	Mn3–O13	1.940 (5)
Mn1–O21	1.946 (5)	Mn3–O15	1.968 (5)
Mn1–O23	2.225 (5)	Mn3–O29	2.228 (4)
Mn1–O27	2.156 (5)	Mn3–O31	2.209 (5)
Mn2–O5	1.847 (5)	Mn4–O6	1.840 (5)
Mn2–O9	2.226 (5)	Mn4–O17	2.178 (5)
Mn2–O11	2.173 (5)	Mn4–O19	2.224 (5)
Mn2–O25	1.939 (5)	Mn4–O33	1.931 (5)
Mn2–O42	1.924 (5)	Mn4–O51	1.937 (5)
Mn2–N35	2.054 (6)	Mn4–N44	2.062 (6)

b. Angles

Mn1–O5–Mn2	124.6 (2)	Mn1–O5–Mn3	96.9 (2)
Mn2–O5–Mn3	130.2 (2)	Mn1–O6–Mn3	96.9 (2)
Mn1–O6–Mn4	129.1 (2)	Mn3–O6–Mn4	125.4 (2)
O5–Mn1–O6	82.0 (2)	O5–Mn2–O9	93.2 (2)
O5–Mn1–O7	98.2 (2)	O5–Mn2–O11	90.8 (2)
O5–Mn1–O21	172.8 (2)	O5–Mn2–O25	98.2 (2)
O5–Mn1–O23	89.0 (2)	O5–Mn2–O42	171.8 (2)
O5–Mn1–O27	92.0 (2)	O5–Mn2–N35	91.5 (2)
O6–Mn1–O7	173.0 (2)	O9–Mn2–O11	169.2 (2)
O6–Mn1–O21	94.4 (2)	O9–Mn2–O25	89.5 (2)
O6–Mn1–O23	99.0 (2)	O9–Mn2–O42	86.8 (2)
O6–Mn1–O27	87.7 (2)	O9–Mn2–N35	85.1 (2)
O7–Mn1–O21	86.1 (2)	O11–Mn2–O25	99.8 (2)
O7–Mn1–O23	88.0 (2)	O11–Mn2–O42	87.9 (2)
O7–Mn1–O27	85.3 (2)	O11–Mn2–N35	84.8 (2)
O21–Mn1–O23	85.5 (2)	O25–Mn2–O42	90.0 (2)
O21–Mn1–O27	94.0 (2)	O25–Mn2–N35	169.2 (2)
O23–Mn1–O27	173.3 (2)	O42–Mn2–N35	80.4 (2)
O5–Mn3–O6	82.1 (2)	O6–Mn4–O17	93.1 (2)
O5–Mn3–O13	94.3 (2)	O6–Mn4–O19	93.4 (2)
O5–Mn3–O15	173.7 (2)	O6–Mn4–O33	96.4 (2)
O5–Mn3–O29	88.0 (2)	O6–Mn4–O51	172.3 (2)
O5–Mn3–O31	96.6 (2)	O6–Mn4–N44	91.7 (2)
O6–Mn3–O13	175.7 (2)	O17–Mn4–O19	170.8 (2)
O6–Mn3–O15	96.9 (2)	O17–Mn4–O33	93.6 (2)
O6–Mn3–O29	90.2 (2)	O17–Mn4–O51	86.7 (2)
O6–Mn3–O31	88.1 (2)	O17–Mn4–N44	84.4 (2)
O13–Mn3–O15	86.9 (2)	O19–Mn4–O33	92.0 (2)
O13–Mn3–O29	92.1 (2)	O19–Mn4–O51	86.0 (2)
O13–Mn3–O31	89.9 (2)	O19–Mn4–N44	88.9 (2)
O15–Mn3–O29	85.8 (2)	O33–Mn4–O51	91.4 (2)
O15–Mn3–O31	89.6 (2)	O33–Mn4–N44	171.8 (2)
O29–Mn3–O31	174.9 (2)	O51–Mn4–N44	80.6 (2)

Magnetochemistry. The effective moment of complex **1** as a function of temperature is shown in Figure 3. The value for μ_{eff} gradually decreases from 7.98 μ_B at 300.0 K to 6.35 μ_B at 25.00 K, whereupon the moment falls sharply to 3.28 μ_B by 5.00 K. The high-temperature data are very similar to those observed[5] for $[Mn_4O_2(O_2CMe)_7(bpy)_2](ClO_4)\cdot 3H_2O$, but the latter complex did not display a rapid decrease in μ_{eff} at low temperatures. As we have reported previously,[5,16] the spin Hamiltonian appropriate for a tetranuclear butterfly arrangement of metal ions is given by eq 3, where we have adhered to the crystallographic numbering

$$\hat{H} = -2J_{12}\hat{S}_1\cdot\hat{S}_2 - 2J_{23}\hat{S}_2\cdot\hat{S}_3 - 2J_{34}\hat{S}_3\cdot\hat{S}_4 - 2J_{41}\hat{S}_4\cdot\hat{S}_1 - 2J_{13}\hat{S}_1\cdot\hat{S}_3 \quad (3)$$

scheme indicated in Figure 1. The Hamiltonian in eq 3 assumes that all pairwise interactions in the molecule are unique. However, based on an analysis of the structure of complex **1**, it is reasonable to simplify eq 3 to

$$\hat{H} = -2J_{wb}(\hat{S}_1\cdot\hat{S}_2 + \hat{S}_2\cdot\hat{S}_3 + \hat{S}_3\cdot\hat{S}_4 + \hat{S}_4\cdot\hat{S}_1) - 2J_{bb}\hat{S}_1\cdot\hat{S}_3 \quad (4)$$

where we have approximated all of the butterfly "wing-to-body" interactions about the periphery of the complex as being equal (i.e., $J_{wb} = J_{12} = J_{23} = J_{34} = J_{41}$). The "body-to-body" interaction parameter J_{13} is renamed as J_{bb}. Within the framework of the model described by eq 4, it is possible to generate an operator-equivalent expression by using the Kambe method of momentum coupling:[17]

$$\hat{H} = -J_{wb}(\hat{S}_T^2 - \hat{S}_A^2 - \hat{S}_B^2) - J_{bb}\hat{S}_A^2 \quad (5)$$

This equation was obtained by a vector coupling of spin operators where $\hat{S}_A = \hat{S}_1 + \hat{S}_3$, $\hat{S}_B = \hat{S}_2 + \hat{S}_4$, and $\hat{S}_T = \hat{S}_A + \hat{S}_B$. The corresponding eigenvalue expression is given by

$$E = -J_{wb}[S_T(S_T + 1) - S_A(S_A + 1) - S_B(S_B + 1)] - J_{bb}[S_A(S_A + 1)] \quad (6)$$

A total of 85 spin states with S_T values ranging from 0 to 8 are generated by eq 6 for a tetranuclear complex of high-spin Mn^{III} ions ($S = 2$).

Attempts to fit the data in Figure 3 with the derived susceptibility expression employing the eigenvalues of the 85 spin states from eq 6 mimicked the overall decrease in μ_{eff} with decreasing temperature and suggested an $S = 3$ ground state. However, the theoretical curve failed to reproduce the sharp drop in μ_{eff} below 25.00 K. Equation 6 was thus modified to allow for zero-field splitting of the $S = 3$ ground state with the addition of the Hamiltonian in eq 7, where D is the axial zero-field-splitting

$$\hat{H} = D(\hat{S}_z^2 - \tfrac{1}{3}\hat{S}_T^2) \quad (7)$$

parameter for the $S = 3$ ground state. The solid line in Figure 3 represents the best fit to the zero-field-splitting model with $g = 1.96$, $J_{wb} = -5.3$ cm^{-1}, $J_{bb} = -24.6$ cm^{-1}, and $D = 3.7$ cm^{-1}; contribution from temperature-independent paramagnetism (TIP) was held fixed at 2.00×10^{-4} cgsu. The data clearly fit this model reasonably well, with the positive value of D indicating a net stabilization of the $m_s = 0$ component of the ground state. In Figure 4 is shown a plot of the relative error for fitting the data

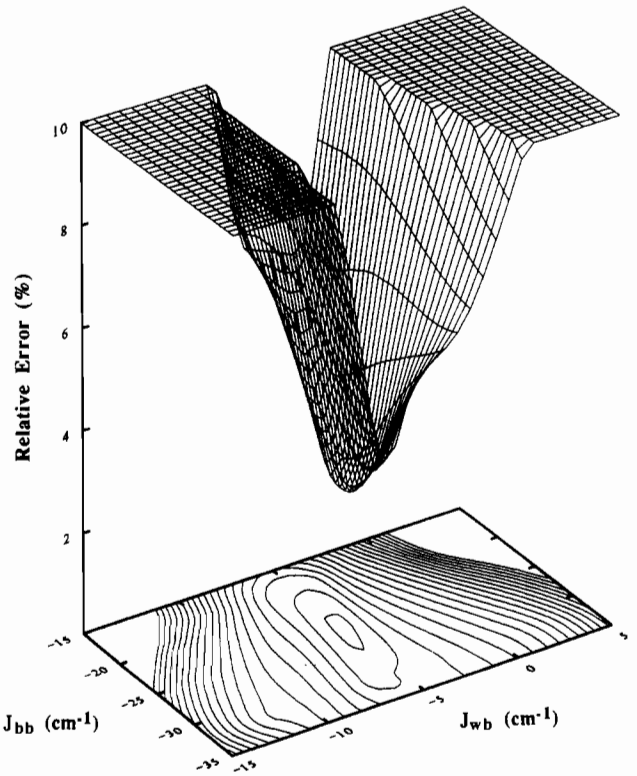

Figure 4. Plot of the relative error surface for fitting the susceptibility data of $(NBu^n_4)[Mn_4O_2(O_2CMe)_7(pic)_2]$ (**1**) as a function of the coupling parameters J_{wb} and J_{bb} for $g = 1.96$ and $D = 3.7$ cm^{-1}. In the bottom of the figure is shown a two-dimensional contour projection of the surface.

(16) McCusker, J. K.; Vincent, J. B.; Schmitt, E. A.; Mino, M. L.; Shin, K.; Coggin, D. K.; Hagan, P. M.; Huffman, J. C.; Christou, G.; Hendrickson, D. N. *J. Am. Chem. Soc.* **1991**, *113*, 3012.

(17) Kambe, K. *J. Phys. Soc. Jpn.* **1950**, *5*, 48.

for complex **1** as a function of both J_{wb} and J_{bb}. This surface was calculated for $g = 1.96$ and $D = 3.7$ cm^{-1}. It can be concluded from this diagram that the above parameters do represent a well-defined minimum for this system and allow us to estimate the error bars on the quoted J values as approximately ± 0.5 cm^{-1}.

It should be pointed out that, while a good fit of the data was obtained by adding an axial zero-field-splitting parameter D for the $S = 3$ ground state (Figure 3), it is not expected that this D value is very accurately determined. From bulk susceptibility data it is not possible to determine D values with accuracy. In addition, the values of J_{wb} and J_{bb} found for complex **1** indicate that there are several excited states (including one with $S_T = 4$) within 15 cm^{-1} of the ground state. Fortunately, the values of J_{wb} and J_{bb} are not very dependent on the value of D taken for the ground state.

Intermediate-Spin Ground State and Spin Frustration. The spin operator coupling used to derive eq 6 makes it possible to identify not only the total spin of a given state but also the relative magnitudes of the single-ion spin operator components. This is extremely useful in describing the nature of a given state, particularly for complexes in which there exist multiple coupling pathways of similar sign and magnitude, as well as systems having several states with the same total spin. For example, in the case of complex **1**, there are 17 different states all having $S_T = 3$. In generating the various $\hat{S}_A$, $\hat{S}_B$, and $\hat{S}_T$ values to be used in the eigenvalue eq 6, the rules governing vector addition are followed. Two spin vectors such as $\hat{S}_1$ and $\hat{S}_3$, when combined vectorially, yield values for their sum that span $|S_1 + S_3|, ..., |S_1 - S_3|$ in integer steps. Thus, for $S_1 = S_3 = 2$, the vector $\hat{S}_A$ can take on any integer value from 0 to 4. In terms of the nature of the exchange interaction responsible for the vector $\hat{S}_A$, a value of 0 indicates an antiferromagnetic alignment of the single-ion vectors while $S_A = 4$ represents a parallel (ferromagnetic) alignment of spins. The $S = 3$ ground state in complex **1** has component $\hat{S}_A$ and $\hat{S}_B$ values of 1 and 4, respectively. The ground state is characterized by $S_T = 3$, which is intermediate between the two possible extremes of 0 and 8. The value of $\hat{S}_B$, although indicating a parallel alignment of the spin vectors on Mn2 and Mn4, is not indicative of any intrinsic spin–spin interaction between these metal ions, since we have assumed in eq 3 that the interaction between these ions is negligible (i.e., $J_{24} = 0$). However, the value of $\hat{S}_A$ is diagnostic of the Mn1···Mn3 interaction. As indicated, the vectorial coupling of $\hat{S}_1$ and $\hat{S}_3$ gives $\hat{S}_A$, which can have the values 0, 1, 2, 3, and 4. These values for $\hat{S}_A$ can be viewed as resulting from different relative orientations of $\hat{S}_1$ and $\hat{S}_3$, which can be schematically represented as follows:

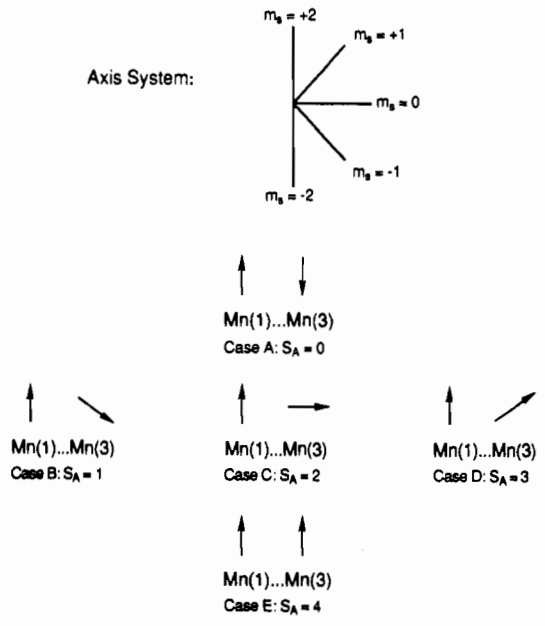

The Mn1···Mn3 interaction present in complex **1** is represented by case B. The fact that $J_{bb} < 0$ indicates that the natural tendency of the Mn1···Mn3 interaction is to achieve an antiparallel alignment of the $\hat{S}_1$ and $\hat{S}_3$ spin vectors, i.e., case A. The reason that an intermediate vector sum is produced is due to the presence of the J_{wb} interactions. The antiferromagnetic nature of J_{wb}, while weaker than the J_{bb} interaction, is still sufficiently strong (vide infra) to prevent the spin vectors comprising $\hat{S}_A$ from completely pairing up. The result is a partial offsetting of the antiferromagnetic nature of the J_{bb} interaction and an intermediate value for the vector sum $\hat{S}_A$. This situation, where competing exchange pathways result in deviations from the intrinsic character of a given exchange interaction, is called spin frustration.

Spin frustration is not a new concept; it has been recognized for a variety of extended magnetic systems.[18] However, its application to the magnetochemistry of discrete polynuclear complexes is not widely recognized.[19] The most easily understood example of spin frustration in a discrete complex is provided by the μ_3-oxide-bridged triangular complexes of the general formula $[M_3O(O_2CR)_6L_3]$, where L is some ligand such as pyridine. As was noted above, the structure of complex **1** can actually be viewed as two triangular Mn_3O units sharing a common edge. To shed more light on the origin of the magnetic structure of complex **1** as well as explain in more detail our view of spin frustration, it is instructive to examine from a theoretical standpoint the magnetic structure of a triangular high-spin Mn^{III} complex. In order to provide a more ready comparison with complex **1**, we consider an isosceles arrangement of metal ions

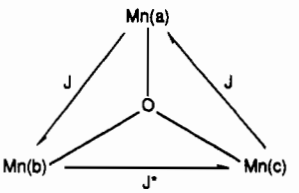

where J corresponds to J_{wb} and J^* to J_{bb}. The operator-equivalent Hamiltonian describing this spin system is given by eq 8, where

$$\hat{H} = -J(\hat{S}_T^2 - \hat{S}_{bc}^2) - J^*\hat{S}_{bc}^2 \quad (8)$$

$\hat{S}_T = \hat{S}_{bc} + \hat{S}_a$ and $\hat{S}_{bc} = \hat{S}_b + \hat{S}_c$. Nineteen states with S_T values ranging from 0 to 6 are found for this spin system.

In Figure 5 are shown the eigenvalues of eq 8 as a function of the ratio J/J^*. This figure was generated by assuming $J < 0$ and $J^* < 0$; i.e., both exchange pathways are antiferromagnetic. The most useful way of interpreting this figure is to equate movement along the x axis as a means of varying the level of spin frustration present in the complex. If the J^* interaction is much stronger than the J interaction, the frustration of the J pathway is complete and the spin vectors on Mn(b) and Mn(c) will pair to give a resultant of 0. The spin of the ground state then results solely from Mn(a), which in the present case gives $S_T = 2$. As the relative magnitude of J increases, an $S_T = 1$ state characterized by $\hat{S}_{bc} = 1$ becomes the ground state. The J^* interaction is still dominant for $J/J^* < 1$, but now the J pathway is sufficiently strong to prevent a complete pairing of the spins on Mn(b) and Mn(c). This is exactly analogous to the situation found in complex **1**. In fact, if one interpolates the J/J^* ratio found from the analysis of complex **1** on the eigenvalue diagram in Figure 5, it is found that the J values are close to an $S_T = 1$ state for each Mn_3O fragment. Combining the two $S = 1$ triangular fragments by edge-sharing will yield an $S = 3$ ground state due to the

(18) $CsCoCl_3$, a quasi-one-dimensional antiferromagnet, is the first compound studied in connection with spin frustration in an ordered lattice: (a) Mekata, M.; Adachi, K. *J. Phys. Soc. Jpn.* **1978**, *44*, 806–812. More recent references: (b) Tanaka, M.; Iwasaki, H.; Siratori, K.; Shindo, I. *J. Phys. Soc. Jpn.* **1989**, *58*, 1433–1440. (c) Mekata, M.; Ajiro, Y.; Adachi, K. *J. Magn. Magn. Mater.* **1986**, *54–57*, 1267–1268. (d) Farneth, W. E.; McLean, R. S.; McCarron, E. M.; Zuo, F.; Lu, Y.; Patton, B. R.; Epstein, A. *J. Phys. Rev. B* **1989**, *39*, 6594.

(19) McCusker, J. K.; Schmitt, E. A.; Hendrickson, D. N. In *Magnetic Molecular Materials*; Gatteschi, D., Ed.; Kluwer Academic Publishers: Dordrecht, The Netherlands, in press.

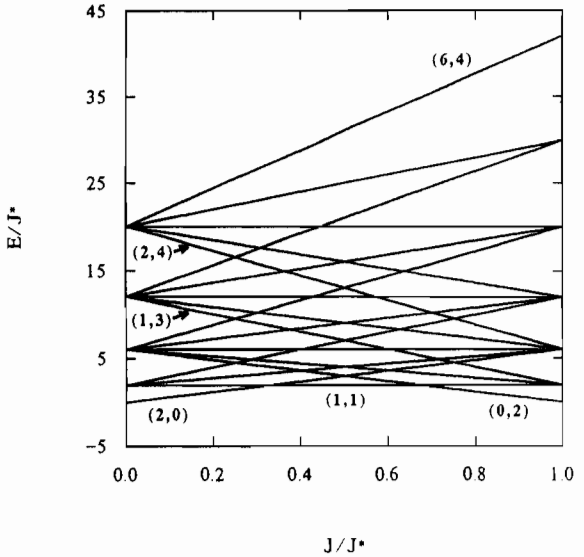

Figure 5. Plot of the eigenstates of eq 8 for a triangular Mn^{III}_3O complex. The states are labeled in terms of (S_T,S_{bc}). See the text for details.

effective pairing of spins that occurs between the two wing-tip ions:

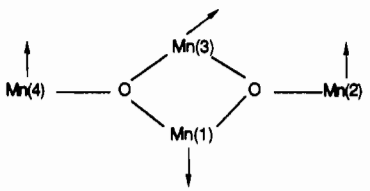

As $J/J^* \to \infty$ is further increased for the triangular complex, an $S_T = 0$ ground state is produced. The value of $S_{bc} = 2$ indicates a larger deviation from the expected value of 0 based solely on the nature of the J^* interaction. This canting of the spin vectors away from their preferred antiparallel alignment and the production of intermediate vector couples are a direct consequence of the larger J interaction. At values of $J/J^* > 1$, the S_T value of the ground state begins increasing again, but now with values for $\hat{S}_{bc}$ that resemble a canting from a ferromagnetic alignment rather than from an intrinsically antiferromagnetic interaction. Finally, when $J \gg J^*$, an $S_T = 2$ ground state is found for which $\hat{S}_{bc} = 4$. This, of course, is the maximum value that $\hat{S}_{bc}$ can have. This regime represents the opposite extreme from the other $S_T = 2$ ground state. That is, this second $S_T = 2$ state is characterized by a complete frustration of the J^* pathway and a ferromagnetic alignment of $\hat{S}_b$ and $\hat{S}_c$ despite the fact that $J^* < 0$.

The region about $J/J^* = 1$ is of particular interest. When $J = J^*$, eq 8 collapses to

$$\hat{H} = -J\hat{S}_T^2 \qquad (9)$$

where $\hat{S}_T = \hat{S}_a + \hat{S}_b + \hat{S}_c$. The spin Hamiltonian of eq 9 describes an equilateral arrangement of ions where none of the three pairwise interactions are dominant. Although from Figure 5 it is found that the ground state is $S_T = 0$ in this instance, it is not obvious that this should be the case. In fact, it is difficult to predict a priori what the most stable state should be for an equilateral array of spin vectors. This question also relates to the origin of the particular combination of $\hat{S}_A$ and $\hat{S}_B$ that produces the ground state in complex **1**. At this point, the origin of the $\hat{S}_A$ and $\hat{S}_B$ terms is clear. But why should the ground state be described by the *difference* $|S_A - S_B|$ as opposed to the sum $|S_A + S_B|$? On the basis of the above analysis of the Mn_3O system as well as similar analyses on Fe^{III}_3O,[20] $Mn^{III}_2Mn^{II}O$, $Fe^{III}_2Fe^{II}O$, and V^{III}_3O systems,[21] the following empirical observations can be made: (a) for a given polynuclear spin system, a relatively wide range of spin states are accessible even though all of the pairwise exchange interactions may be intrinsically antiferromagnetic; (b) the relative magnitudes of competing coupling pathways are critically important in determining not only the S value of the ground state but also the nature of the component spin vectors; and (c) when competing exchange pathways are antiferromagnetic and are of similar magnitude, the complex will have a ground state with the smallest possible S value. For a symmetric triangular array of Mn^{III} ions where $J < 0$, the ground state tends toward a state of *minimum* unpaired spin density, or $S_T = 0$. A similar result is found theoretically[20] and is known experimentally for $[Fe_3O(O_2CR)_6L_3]$ complexes,[22] where $S = {}^1/_2$ ground states have been found in all cases studied to date.[23]

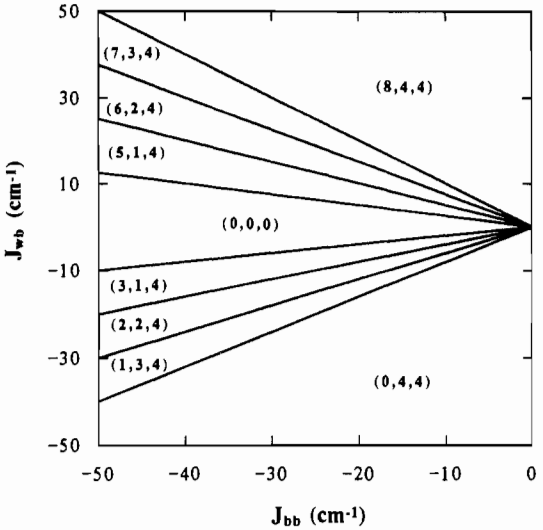

Figure 6. Ground-state boundary delineations for a $[Mn_4O_2]^{8+}$ core. States are labeled as (S_T,S_A,S_B).

The influence these various factors have on the possible ground states of $[Mn_4O_2]^{8+}$ core structures can be gleaned from Figure 6. In this figure is a plot of the possible ground states for a molecule such as complex **1** as a function of the two coupling constants J_{wb} and J_{bb}. It can be seen that the ground state of complex **1** represents the largest spin ground state possible for this system when both interactions are antiferromagnetic. It should be noted that the various ground states in this quadrant differ only in the value of $\hat{S}_A$. In analogy to the discussion above and what is shown in Figure 5, movement along either an x-axis or y-axis trajectory can be thought of in terms of varying the degree of spin frustration present in the tetranuclear core. In particular, movement along the y axis at constant x provides a means of stepping $\hat{S}_A$ through all of its possible values from 0 to 4. This variation is due solely to the relative magnitude of the J_{wb} exchange parameter. What should become apparent from this figure, however, is that substantial changes in the S value of the ground state can come about from relatively minor changes in the strengths of the various interactions. The total spin of the system does appear to be much more sensitive to the value of J_{wb} than the value of J_{bb}. However, this is quite reasonable, considering that there are actually four pairwise interactions described by J_{wb} as opposed to only one for J_{bb}. What this means in terms of spin frustration is that the disparity between J_{wb} and J_{bb} must be

(20) (a) Harvey, D. F.; Christmas, C. A.; McCusker, J. K.; Hagan, P. M.; Chadha, R. K.; Hendrickson, D. N. *Angew. Chem., Int. Ed. Engl.* **1991**, *30*, 598. (b) McCusker, J. K.; Christmas, C. A.; Hagan, P. M.; Chadha, R. K.; Harvey, D. F.; Hendrickson, D. N. *J. Am. Chem. Soc.*, in press.

(21) McCusker, J. K.; Hendrickson, D. N. Unpublished results.

(22) Cannon, R. D.; White, R. P. *Prog. Inorg. Chem.* **1988**, *36*, 195–298 and references therein.

(23) (a) A $S = {}^5/_2$ ground state has been found for one μ_3-O Fe^{III}_3 complex; see: Gorun, S. M.; Papaefthymiou, G. C.; Frankel, R. B.; Lippard, S. J. *J. Am. Chem. Soc.* **1987**, *109*, 4244. (b) In addition to HDVV exchange interactions, the splitting of the spin states in these complexes will also reflect a variety of other effects such as antisymmetric and quadratic exchange and spin–orbit splitting interactions: Tsukerblat, B. S.; Belinskii, M. I.; Fainzil'berg, V. E. *Sov. Sci. Rev., Sect. B* **1987**, *9*, 337.

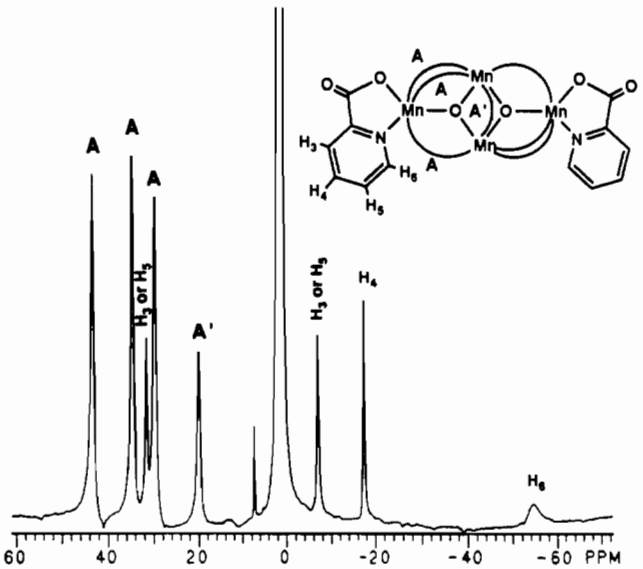

Figure 7. Proton NMR spectrum of complex **1** in $CDCl_3$. The peaks are labeled according to the scheme shown as an inset. The band of resonances in the 0–5 ppm region is from $NBu^n_4{}^+$ protons; the peak at 7.26 ppm is from residual $CHCl_3$ in the solvent.

substantially in favor of the latter before any offsetting of the J_{wb} interaction will occur. Conversely, a fairly small J_{wb}/J_{bb} ratio would be required to begin seeing the effects of spin frustration in the spin polarization of the J_{bb} ions. This is the situation present in complex **1**, where a ratio of ≈ 0.2 is sufficient to produce an intermediate value of $\hat{S}_A$.

In terms of combining $\hat{S}_A$ and $\hat{S}_B$ to form the ground state, one can see from Figure 6 that the general principle discussed above regarding the nature of the various interactions holds here as well. For all values of J_{wb} and $J_{bb} < 0$, the ground state is described by the *difference* of S_A and S_B. Even though the value of S_A is being modified by the relative magnitudes of the two competing interactions, the total spin system is still tending toward a state of minimum unpaired spin density, i.e., $S_T = |S_A - S_B|$. Once the sign of the J_{wb} interaction changes, however, this tendency is reversed. The ground state is now describable in terms of the *maximum* spin available based on values for S_A and S_B, or $S_T = |S_A + S_B|$. This tendency is present even though the J_{bb} interaction is still antiferromagnetic; this relates back to the fact that the spin system comprises four J_{wb} interactions.

Proton NMR Spectroscopy. An NMR investigation of complex **1** has been carried out to complement that previously reported for $[Mn_4O_2(O_2CMe)_7(bpy)_2](ClO_4)\cdot 3H_2O$.[5] Complex **1** has a large magnetic moment at room temperature (ca. 8 μ_B), and the proton resonances are thus very broadened and shifted from their diamagnetic positions. Nevertheless, as shown in Figure 7, the resonances were clearly located and are well resolved. In $CDCl_3$, eight ligand peaks are observed, and this corresponds exactly to the number expected for a molecule with idealized C_2 symmetry: four resonances from four inequivalent $MeCO_2^-$ groups and four resonances from the pic protons. The spectrum thus supports retention in solution of the solid-state structure of **1**. The resonance positions are listed in Table IV, using the proton-labeling scheme shown in Figure 7.

The assignments in Figure 7 and Table IV were made by a combination of the following: (i) preparation of the $CD_3CO_2^-$ version of **1**, which allowed ready identification of the acetate resonances in Figure 7 as those that are not present in the spectrum of the deuterated version; and (ii) consideration of peak widths at half height ($\nu_{1/2}$), which allowed identification of H_6 and H_4 peaks, the broadest and narrowest aromatic proton resonances, respectively, consistent with their relative distances from the paramagnetic metal centers. The remaining two resonances are assigned as the H_3/H_5 protons. As expected, the broadness of the proton resonances ($\nu_{1/2}$) is inversely proportional to the spin–lattice relaxation (T_1) times as measured by the inversion recovery method (Table IV). The four acetate peaks have similar $\nu_{1/2}/T_1$ values, and their approximately 2:2:2:1 intensity ratio thus indicates the peak at 19.9 ppm (A′) to be that of the unique acetate bridging the central ("body") Mn atoms, Mn1 and Mn3. The resonance positions of the acetate protons in **1** are all within 3–4 ppm of those for $[Mn_4O_2(O_2CMe)_7(bpy)_2]^+$, consistent with the similarity in the two structures and the near-equal magnitudes of the intramolecular magnetic exchange interactions. The resonance positions of the aromatic protons in **1** are more different from those in the bpy complex; however, this is consistent with the different nature of pic vs bpy. Similarities exist, nevertheless, particularly the upfield shift of the H_6 and H_4 resonances from their diamagnetic positions in both complexes. The observation for the pic protons of both upfield and downfield shifts from diamagnetic resonance positions is evidence for a contribution to the isotropic shifts from a π-spin-delocalization mechanism;[24] similar behavior was observed for the bpy complex, where it was discussed in more detail and a π contribution was supported by the spectrum of the corresponding Me-substituted bpy complex.[5]

Table IV. Proton NMR Data for Complex **1** in $CDCl_3$ at 23 °C

shift, ppm[a]	$\nu_{1/2}$, Hz[b]	T_1, ms[c]	assgnt[e]
43.1	137	2.3	acetate (A)
34.4	135	2.2	acetate (A)
31.5 (31.6)	77	3.0	H_3/H_5
29.6	146	1.9	acetate (A)
19.9	129	2.3	acetate (A′)[d]
−6.8 (−7.0)	71	4.3	H_3/H_5
−17.2 (−17.0)	48	8.3	H_4
~−54 (−54)	~660	<1	H_6

[a] Vs $SiMe_4$; downfield shifts are designated as positive (δ scale); values in parentheses are for the deuterated complex. [b] Peak width at half-height. [c] Inversion recovery method. [d] Unique acetate (A′) bridging Mn1 and Mn3. [e] Numbering of pic protons as in Figure 7.

It is instructive to compare and contrast the spectra obtained for complex **1** and $[Mn_4O_2(O_2CMe)_7(bpy)_2](ClO_4)\cdot 3H_2O$ with the spectrum of the complex $[Fe_4O_2(O_2CMe)_7(bpy)_2](ClO_4)$.[16] In all three cases, the number of peaks is as expected if C_2 symmetry is assumed for the metal-containing ions. However, there are some important differences regarding the details of the spectra that should be mentioned. First, the Mn complexes display downfield shifts for their acetate resonances from diamagnetic positions but both downfield and upfield shifts for their aromatic protons; in contrast, all shifts in the Fe complex either are downfield or are essentially at (bpy 4,4′) their diamagnetic positions. Second, the peaks for the Mn complexes occur over a much greater range (+45 to −131 ppm) than those in the Fe complex (+38 to +6); this is consistent with the weaker paramagnetism of the latter ($\mu_{eff} \approx 4.20\ \mu_B$) compared with the former (ca. 8 μ_B). Third, the chemical shifts of the protons at equivalent ring positions in the two halves of the bpy molecule are more similar for $[Fe_4O_2(O_2CMe)_7(bpy)_2]^+$ than for the Mn complex. For example, the 6,6′ and 4,4′ bpy protons have chemical shift *differences* of (Fe) 4.50 and 0.58 ppm, respectively and (Mn) 54.6 and 11.2 ppm, respectively. These are dramatic differences, even if one allows for the greater isotropic shifts in the Mn complex. This behavior can be rationalized as resulting from the more symmetric distribution of unpaired electron density for high-spin d^5 (Fe^{III}) vs high-spin d^4 (Mn^{III}). Differing unpaired spin density in the e_g orbitals will be reflected in observed spectra because this will influence the contribution to the observed isotropic shifts from a σ-spin-delocalization mechanism. The Mn pic complex **1** does not display this effect because of the nature of the pic ligand, but this effect of the symmetry of electron distribution on the NMR chemical shift distribution is an important one to remember as this spectroscopic technique is applied to future examples of M_4O_2 or related species.

The proton NMR spectra of complex **1** have also been recorded in CD_3CN and $(CD_3)_2SO$, with two objectives in mind: first, to

(24) *NMR of Paramagnetic Molecules*; LaMar, G. N., Horrocks, W. DeW., Jr., Holm, R. H., Eds.; Academic Press: New York, 1973.

Table V. Solvent Dependence[a] of the Proton NMR Spectrum of Complex **1** at 25 °C

resonance	δ, ppm $CDCl_3$	CD_3CN	$(CD_3)_2SO$
acetate (A)	43.3	42.7	43.0
acetate (A)	34.6	33.9	34.3
H_3/H_5	31.6	30.6	30.2
acetate (A)	29.7	29.7	29.5
acetate (A′)	20.0	20.1	20.2
H_3/H_5	−6.8	−8.6	−9.4
H_4	−17.2	−19.5	−19.3
H_6	∼−54	∼−62	∼−63

[a] at equivalent concentrations (11.4–11.8 mM).

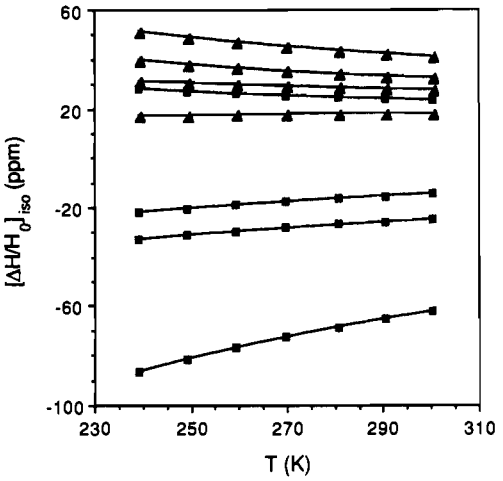

Figure 8. Temperature dependence of the isotropic shifts $(\Delta H/H_0)_{iso}$ for complex **1** in $CDCl_3$. The solid lines are present as a visual aid.

investigate whether the tetranuclear anion of **1** maintains its structural integrity in the better donor solvents and, second, to document the extent of solvent dependence of the resonance positions for distinctly different solvents. The results of this investigation are tabulated in Table V. The three spectra are very similar in appearance vis-à-vis the number of peaks, their broadness, and their resonance positions. Only minor variations in chemical shift are apparent in Table V, the most solvent-dependent resonance being that of the H_6 protons. We conclude that the anion of **1** does maintain its structural integrity in good donor solvents, and the proton resonance positions are only slightly solvent dependent. The former conclusion is supported by a Beer's law dependence study in DMSO; a linear dependence (R = 0.996–0.999) of absorption vs concentration was observed at three wavelengths (500, 550, 600 nm) in the concentration range 10^{-3}–10^{-4} M.

The temperature dependence of the NMR spectrum has been investigated in $CDCl_3$ in the temperature range 239.0–300.3 K. In Figure 8 are summarized the results of this study. The data are plotted as isotropic shift $(\Delta H/H_0)_{iso}$ vs temperature, where $(\Delta H/H_0)_{iso}$ is the shift (ppm) of a resonance from its position in a diamagnetic compound; the chemical shifts of the free ligands were employed in this case.[25] It is apparent from Figure 8 that the resonance positions are distinctly temperature dependent, with the H_6 protons displaying the greatest dependence, approximately 24 ppm variation over 60 K. With one exception, the isotropic shifts increase in magnitude with decreasing temperature. This parallels the variation of χ_m with T, consistent with contact shifts via σ/π spin delocalization mechanisms. The resonance of the unique bridging acetate (A′) is, however, only slightly temperature dependent (0.91 ppm over 60 K), and its isotropic shift *decreases* with decreasing temperature.

(25) Chemical shifts employed (ppm vs TMS): CH_3COOH 2.05; picH H_3 8.27, H_4 7.98, H_5 7.62, H_6 8.77. To calculate the isotropic shifts of the H_3/H_5 protons, the average (7.95 ppm) of the free-ligand values was used.

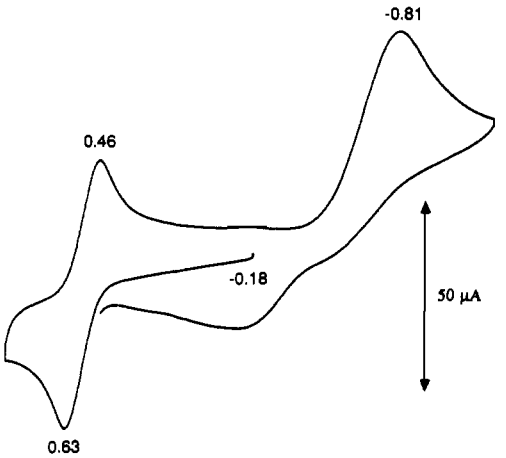

Figure 9. Cyclic voltammogram (100 mV/s) for complex **2** in CH_2Cl_2. The quoted potentials (V) are vs ferrocene/ferrocenium.

The position in the molecule of the unique acetate (A′) leads to its being the only one to have both its carboxylate oxygen atoms (O27 and O29) occupying axially elongated positions of the Jahn–Teller distortion. This made us suspect that it might be significantly more labile than the other acetate groups, and we have explored this in a simple qualitative manner using NMR spectroscopy. Addition of a few equivalents of CD_3CO_2D to the NMR solution in $CDCl_3$ led to complete disappearance of the 19.9 ppm peak while influencing the other acetate resonances only very slightly; a new resonance at ∼10.5 ppm appeared, assigned to an averaged environment of the free and bound $CH_3CO_2^-$ groups. This result demonstrates fast exchange, on the proton NMR time scale, of the unique A′ acetate with free acetic acid, consistent with the location of this ligand.

Electrochemistry. The cyclic voltammograms (CV's) of complexes **1** and **2** have been recorded in CH_2Cl_2 solution. Both complexes give similar results; the CV of **2** is shown in Figure 9. Both complexes display a quasi-reversible one-electron oxidation, at $E_{1/2}$ values of 0.52 and 0.54 V vs ferrocene for **1** and **2**, respectively. The peak separations are 180 and 170 mV, respectively, both similar to that measured separately for the ferrocene/ferrocenium couple (190 mV) under similar conditions (no iR compensation employed). The i_a/i_c ratio is ∼1 or just below. For the oxidation processes of both complexes, plots of i_p vs $v^{1/2}$ gave straight lines in the scan rate (v) range of 50–500 mV/s, indicating a diffusion-controlled process. Both complexes also display an irreversible reduction, at peak potentials of −0.86 and −0.81 V, respectively. There are also some additional, very broad and grossly irreversible features at peak potentials of ∼1 V and −1.3 to −1.8 V. These are better defined in differential-pulse voltammograms, but are again very broad. In MeCN, the same overall behavior is observed, the main difference being that the oxidation process becomes less reversible, as judged by the i_a/i_c values, which become significantly less than 1. This may, however, be due, at least in part, to the nearby second (irreversible) oxidation at ∼1 V. The reverse current for the first oxidation process is very sensitive to the switching potential, increasing significantly if the scan is reversed before the second process; the same is also true, in fact, in CH_2Cl_2 solution. Linear i_p vs $v^{1/2}$ plots were again obtained for both complexes in MeCN.

The quasi-reversible oxidation at 0.54 V for **2** in CH_2Cl_2 (0.69 V in MeCN) is assigned to oxidation to the $3Mn^{III},Mn^{IV}$ level, as shown in eq 10. This oxidation potential can be compared

$$\underset{4Mn^{III}}{[Mn_4O_2(O_2CPh)_7(pic)_2]^-} \overset{0.54\ V}{\rightleftharpoons} \underset{3Mn^{III},Mn^{IV}}{Mn_4O_2(O_2CPh)_7(pic)_2} \quad (10)$$

to that found in CH_2Cl_2 for the corresponding couple in $[Mn_4O_2(O_2CPh)_7(bpy)_2]^+$; the value for the latter vs ferrocene is 0.87 V.[5] Thus, the substitution of bpy by pic causes a decrease in potential of 0.33 V. As described earlier, the bpy/pic substitution has an insignificant effect on the structures of the two complexes or on their magnetic exchange interactions, but the

electrochemical results indicate a significant influence on the redox properties, complex **2** being noticeably easier to oxidize; this is intuitively consistent with the change in overall charge on replacement of neutral bpy with anionic pic^-. A similar observation has been made in dinuclear Mn chemistry. The two species $[Mn_2O_2(tpa)_2]^{3+}$ [26a,b] and $[Mn_2O_2(N_3O\text{-}py)_2]^{+}$ [26c] (tpa = tris(2-pyridylmethyl)amine; N_3O-py = *N*,*N*-bis(2-pyridylmethyl)-glycinate) differ only in having one pyridyl donor group in the former replaced by a carboxylate group; comparison of the electrochemical properties shows that the potentials of the $Mn^{III}_2/Mn^{III}Mn^{IV}$ and $Mn^{III}Mn^{IV}/Mn^{IV}_2$ couples for the two species differ by 0.26 and 0.28 V, respectively, the N_3O-py complex being easier to oxidize in each case.[26b,c] The 0.33-V change in the potential of **2** vs the bpy analogue is thus slightly greater. This is interesting, for only two ligands per four Mn atoms have been changed in the Mn_4O_2 case, whereas two ligands per two Mn atoms have been changed for the dinuclear case. One might have reasonably expected the effect on redox potentials to thus be greater for the Mn_2 species, not the other way around. This suggests that redox potentials of Mn_4O_2 species may be particularly sensitive to and "tunable" by ligand variation, a matter that is currently being investigated by synthesis of additional examples. We believe the above observations to be of relevance to the biological importance of this work, as well be discussed below. Note also that $[Mn_4O_2(O_2CPh)_7(bpy)_2]^+$ undergoes a quasi-reversible *reduction* to the neutral complex (Mn^{II},$3Mn^{III}$), behavior not exhibited by **2** (or **1**).

Discussion

It has been demonstrated in this work that the attainment and stability of complexes containing the $[Mn_4O_2]^{8+}$ core are not limited to the use of bpy, nor are they in some way a consequence of any specific property of this ligand, other than its chelating nature and resistance to oxidation by Mn^{III}. The employment of pic^- leads to products with the same formulation and, as has been described, near-superimposable structures and almost identical magnetic exchange interactions. The primary function of the chelating ligands is almost certainly to preclude formation of trinuclear $[Mn_3O]$-containing complexes, another thermodynamically favorable arrangement and potential product of $Mn^{III}/O/RCO_2^-$ components. However, even this last statement must be qualified, because in more recent work we have managed to isolate $[Mn_4O_2]$-containing species with *no* chelating ligands at all.[27] We conclude that carboxylate-bridged Mn_4O_2 cores are inherently thermodynamically stable entities at the $\sim$+3 metal oxidation level, and while this does not constitute any kind of proof for their involvement within the WOC, it does suggest that they should continue to be entertained as possible candidates for the native structural unit at the lower S_n states.

The observation that the major influence of the pic-for-bpy substitution is to decrease the oxidation potential is particularly interesting. After all, the lower S_n states must be oxidized to higher S_n states before water oxidation can be accomplished, and generation of higher S_n states is driven by, and must therefore be within the oxidizing capability of, the $P680^+$ cation radical formed by charge separation at PSII (more accurately, the native Mn aggregate is oxidized by Z^+, the tyrosine phenoxide radical intermediate between the Mn unit and P680 on the electron-transfer pathway).[2] Whatever the precise details of the $S_1 \rightarrow S_2 \rightarrow S_3$ transitions may be (Mn_4 structures, structural changes accompanying substrate binding, etc.), the observation of lower oxidation potentials in our tetranuclear Mn carboxylate complexes and related dinuclear[26] systems on increasing the carboxylate content and lowering the aromatic amine content is intuitively satisfying, for it provides some rationalization for the data suggesting N (histidine) ligation to the WOC to be minimal.[9] On the basis of the above limited data, the conclusion could be made, as already implied for Mn_2 species,[26c] that the predominantly carboxylate ligation to the WOC Mn_4 aggregate may have been evolutionarily dictated by the need to minimize the oxidation potentials required to access higher oxidation levels (S_n states). With this working hypothesis in mind, we are currently attempting to further increase the O-based ligation in Mn_4O_2 complexes and use additional types of O-containing ligands (chelate or otherwise) to allow further assessment of redox properties and general reactivity characteristics as a function of peripheral ligand nature.

Finally, it is important to comment on the possible biological significance of the $S = 3$ intermediate-spin ground state that we have found for complex **1**. It is clear that spin frustration in these complexes can give rise to a variety of ground states. By reference to Figure 6, it can be seen that a small change in J_{wb} and/or J_{bb} for complex **1** can lead to a ground state characterized by S = 0, 3, 2, or 1. Small changes in the protein structure about the Mn_4^{n+} WOC center could lead to changes in the ground state of the center. It is of interest to note that proteins and enzymes with the $[Fe_4S_4(SR)_4]^{3-}$ active site have been reported[28] to have either $S = {}^1/_2, {}^3/_2, {}^5/_2$, or even larger spin ground states. Recent work[29] on $[Fe_4S_4(SR)_4]^{3-}$ model complexes has established that these complexes show a structural and spin-state variability. In addition to $S = {}^1/_2$ and $S = {}^3/_2$ ground states, these $[Fe_4S_4(SR)_4]^{3-}$ model complexes exhibit ground states characterized either as physical mixtures of $S = {}^1/_2$ and $S = {}^3/_2$ species or as a spin-admixed species. In fact, for the S_2 state of the Mn_4 WOC center, the presence of two EPR signals, one multiline signal at $g \simeq 2$ and another one at $g \simeq 4.1$, has led Brudvig et al. to propose that the two EPR signals arise from two different conformations of a single tetranuclear manganese site.[30] Very recently, Kim et al.[31] showed that the $g \simeq 4.1$ signal does have at least 16 manganese hyperfine lines and therefore is associated with a polynuclear manganese site.

Acknowledgment. This work was supported by NIH Grants GM 39083 (to G.C.) and HL 13652 to (D.N.H.). We thank the Dreyfus Foundation for a Teacher-Scholar Grant (to G.C.).

Supplementary Material Available: Complete listings of atomic coordinates, isotropic and anisotropic thermal parameters, and bond lengths and angles (11 pages); a listing of observed and calculated structure factors (15 pages). Ordering information is given on any current masthead page. A complete MSC structure report (No. 88149) is available on request from the Indiana University Chemistry Library.

(26) (a) Collins, M. A.; Hodgson, D. J.; Michelsen, K.; Towle, D. K. *J. Chem. Soc., Chem. Commun.* **1987**, 1659. (b) Suzuki, M.; Tokura, S.; Suhara, M.; Uehara, A. *Chem. Lett.* **1988**, 477. (c) Suzuki, M.; Senda, H.; Kobayashi, Y.; Oshio, H.; Uehara, A. *Chem. Lett.* **1988**, 1763.

(27) Schake, A. R.; Huffman, J. C.; Folting, K.; Christou, G. Unpublished results.

(28) (a) Lindahl, P. A.; Day, E. P.; Kent, T. A.; Orme-Johnson, W. H.; Münck, E. *J. Biol. Chem.* **1985**, *260*, 11160. (b) Lindahl, P. A.; Gorelick, N. J.; Münck, E.; Orme-Johnson, W. H. *J. Biol. Chem.* **1987**, *262*, 14945. (c) Bertrand, P.; Gayda, J.-P.; Rao, K. K. *J. Chem. Phys.* **1982**, *76*, 4715. (d) Middleton, P.; Dickson, D. P. E.; Johnson, C. E.; Rush, J. D. *Eur. J. Biochem.* **1978**, *88*, 135. (e) Vollmer, S. J.; Switzer, R. L.; Debrunner, P. G. *J. Biol. Chem.* **1983**, *258*, 14284. (f) Huynh, B. H.; Henzl, M. T.; Christner, J. A.; Zimmerman, R.; Orme-Johnson, W. H.; Münck, E. *Biochim. Biophys. Acta* **1980**, *623*, 124. (g) Johnson, M. K.; Thomson, A. J.; Robinson, A. E.; Smith, B. E. *Biochim. Biophys. Acta* **1981**, *671*, 61. (h) Smith, J. P.; Emptage, M. H.; Orme-Johnson, W. H. *J. Biol. Chem.* **1982**, *257*, 2310. (i) Morningstar, J. E.; Johnson, M. K.; Case, E. E.; Hales, B. *J. Biochemistry* **1987**, *26*, 1795. (j) Hagen, W. R.; Wassink, H.; Eady, R. R.; Smith, B. E.; Haaker, H. *Eur. J. Biochem.* **1987**, *169*, 457.

(29) Carney, M. J.; Papaefthymiou, G. C.; Spartalian, K.; Frankel, R. B.; Holm, R. H. *J. Am. Chem. Soc.* **1988**, *110*, 6084.

(30) (a) de Paula, J. C.; Brudvig, G. W. *J. Am. Chem. Soc.* **1985**, *107*, 2643. (b) de Paula, J. C.; Beck, W. F.; Brudvig, G. W. *J. Am. Chem. Soc.* **1986**, *108*, 4002. (c) de Paula, J. C.; Beck, W. F.; Miller, A.-F.; Wilson, R. B.; Brudvig, G. W. *J. Chem. Soc., Faraday Trans. 1* **1987**, *83*, 3635. (d) Beck, W. F.; Brudvig, G. W. *Biochemistry* **1986**, *25*, 6479. (e) de Paula, J. C.; Innes, J. B.; Brudvig, G. W. *Biochemistry* **1985**, *24*, 8114. (f) Brudvig, G. W. In *Advanced EPR, Applications in Biology and Biochemistry*; Hoff, A. J., Ed.; Elsevier: Amsterdam, 1989; p 839.

(31) Kim, D. H.; Britt, R. D.; Klein, M. P.; Sauer, K. *J. Am. Chem. Soc.* **1990**, *112*, 9389.